1-1-2016

Enhanced supercapacitive performances of functionalized activated carbon in novel gel polymer electrolytes with ionic liquid redox-mediated poly(vinyl alcohol)/phosphoric acid

Hyun Seok Jang
Dongguk University

C Justin Raj
Dongguk University

Won-Gil Lee
Dongguk University

Byung Chul Kim
University of Wollongong, bkim@uow.edu.au

Kook Hyun Yu
Dongguk University

Enhanced supercapacitive performances of functionalized activated carbon in novel gel polymer electrolytes with ionic liquid redox-mediated poly(vinyl alcohol)/phosphoric acid

Abstract

Supercapacitors with solid/gel polymer electrolytes have attracted much attention due to their high reliability, flexibility, facile designing, being separator-free and free from electrolyte leakage and volatilization such that they can meet the increasing demands of practical applications. The present work reports on a functionalized activated carbon (AC) supercapacitor based on novel redox-mediated gel polymer electrolyte, PVA/H3PO4/ionic liquid (1-ethyl-3-methylimidazolium tetrafluoroborate, [EMIM]BF4). The electrochemical properties of this supercapacitor were studied using cyclic voltammetry, galvanostatic charge/discharge and electrochemical impedance spectroscopy techniques with various concentrations of [EMIM]BF4 in PVA/H3PO4 gel polymer electrolyte. The incorporation of [EMIM]BF4 in PVA/H3PO4 electrolyte effectively increased the specific capacitance value due to the improved ionic conductivity and additional pseudo-reaction occurring in the electrode/electrolyte interfaces. The specific capacitance of the supercapacitor using PVA/H3PO4/[EMIM]BF4 (50%) electrolyte showed a maximum value of 271 F g-1 at 0.5 A g-1 discharge current, which is much higher than the bare PVA/H3PO4 (103 F g-1) based supercapacitor. The supercapacitor with PVA/H3PO4/[EMIM]BF4 (50%) electrolyte showed enhanced energy and power density of 54.3 W h kg-1 and 23.88 kW kg-1 respectively. Moreover the device showed comparable specific capacitance retention after 3000 cycles of charge/discharge.

Disciplines

Engineering | Physical Sciences and Mathematics

Publication Details

Jang, H., Raj, C. Justin., Lee, W., Kim, B. Chul. & Yu, K. (2016). Enhanced supercapacitive performances of functionalized activated carbon in novel gel polymer electrolytes with ionic liquid redox-mediated poly(vinyl alcohol)/phosphoric acid. RSC Advances, 6 (79), 75376-75383.

Enhanced Supercapacitive Performances of Functionalized Activated Carbon in Novel Gel Polymer Electrolytes with Ionic Liquid redox-mediated Poly(vinyl alcohol)/ Phosphoric Acid

Hyun Seok Jang[a], C. Justin Raj[a*], Won-Gil Lee[a], Byung Chul Kim[a,b] and Kook Hyun Yu[a]*

Supercapacitors with solid/gel polymer electrolytes have attracted much attention due to their high reliability, flexibility, facile designing, separator-free and free from electrolyte leakage and volatilization that can meet the increasing demands of practical applications. The present work reports on a functionalized activated carbon (AC) supercapacitor based on novel redox-mediated gel polymer electrolyte, PVA/H_3PO_4/ionic liquid (1-ethyl-3-methylimidazolium tetrafluoroborate, [EMIM]BF_4). The electrochemical properties of this supercapacitor was studied using cyclic voltammetry, galvanostatic charge/discharge and electrochemical impedance spectroscopy techniques with various concentrations of [EMIM]BF_4 in PVA/H_3PO_4 gel polymer electrolyte. The incorporation of [EMIM]BF_4 in PVA/H_3PO_4 electrolyte effectively increased the specific capacitance value due to the improved ionic conductivity and additional pseudo-reaction occurring in the electrode/electrolyte interfaces. The specific capacitance of the supercapacitor using PVA/H_3PO_4/[EMIM]BF_4(50%) electrolyte showed a maximum value of 271 Fg^{-1} at 0.5 Ag^{-1} discharge current, which is much higher than the bare PVA/H_3PO_4 (103 Fg^{-1}) based supercapacitor. The supercapacitor with PVA/H_3PO_4/[EMIM]BF_4(50%) electrolyte showed enhanced energy and power density of 54.3 $Whkg^{-1}$ and 23.88 $kWkg^{-1}$ respectively. Moreover the device showed comparable specific capacitance retention after 3000 cycles of charge/discharge.

Introduction

Supercapacitors (SC), a kind of reversible electrochemical energy storage system, also known as ultracapacitors or electrochemical capacitors can be a charge/discharge type by physical adsorption/desorption of ions from the electrolyte or through redox reactions occurring at the surface of the positive and negative electrode. Thus it can accumulate a significant amount of energy in a moment and provide current instantaneously or continuously.[1-4] Commercially, supercapacitors based on carbon materials are in high demand owing to their properties like being semi-permanent, eco-friendly, and having high power density compared to the batteries.[5-8] Recently much research has been devoted to improving the energy density of the supercapacitor, so it is gradually replacing the battery in the field of energy storage systems[9-11]. Moreover, the interest in flexible SCs has grown considerably in recent times for fabricating electronics that have bendable displays and wearable electronics, which require flexible electrodes, separator and electrolyte.[12-14]

The SCs based on liquid electrolyte consist of a solid frame with positive/negative electrodes and separator which is filled with liquid electrolytes. These SCs have various practical difficulties due to lack of physical flexibility, so it is hard to be applied to various shapes of electronic devices, and the sturdy exterior surrounding material increases the weight of devices.[15, 16] Moreover, the exterior structure if damaged could result in electrolyte leakage that can cause corrosion of the device and, in addition, organic solvent based liquid electrolytes can even cause explosions. To overcome these difficulties, research on polymer electrolytes has been widely encouraged; since polymer electrolytes can reduce the risk of leakage drastically because of their quasi-solid state form and also afford promising properties like flexibility, elasticity, high ionic conductivity, chemical/electrochemical stability and affinity with the electrodes.[17-19] Moreover, polymer electrolytes can function as a self-separator which can effectively lower the internal resistivity of the cell caused by the separator.[15] The gel polymer electrolyte based on polyvinyl alcohol (PVA)[20, 21], polyvinyl pyrrolidone (PVP)[22], chitosan[16], poly(p-phenylene terephthalamide) (PFTA)[23], polyacrylonitrile (PAN)[24], poly(vinyl chloride) (PVC)[25], polyvinylidene fluoride (PVdF)[26, 27] etc. have been extensively studied and reported; as their conductivity ranges between 10^{-4} to 10^{-3} S cm^{-1} under ambient condition. Among these, common polyvinyl alcohol (PVA) is widely used owing to their attractive properties such as flexibility, elasticity, non-toxicity, biodegradability, and chemical/thermal stabilities. PVA is a water soluble polymer, so its hydrogel can form thin, uniform films as solid electrolyte for SCs. Furthermore, the high dielectric constant, excellent charge storage capacity and dopant-dependent electrical properties make PVA a promising candidate in the development of SCs.

In the recent past, various composites of PVA electrolytes have been fabricated using a mixture of acid, base and salts [28-30]. Even though they show comparable electrochemical

[a.] Department of Chemistry, Dongguk University-Seoul, Seoul-100-715, Republic of Korea. Email: yukook@dongguk.edu; cjustinraj@gmail.com Tel.: +82-2-2260 3709
[b.] ARC Centre of Excellence for Electromaterials Science, IPRI, AIIM Facility, Innovation Campus, University of Wollongong, NSW 2522, Australia
Electronic Supplementary Information (ESI) available: [additional figures]. See DOI: 10.1039/x0xx00000x

performances, the low ionic conductivity (~10 $mScm^{-1}$) cumbers the wide practical applications[31]. So recently, many researchers have introduced a redox-mediated strategy for gel polymer electrolytes for energy storage applications. The quick reversible redox reaction induced by the redox mediator can efficiently enhance the ionic conductivity and add pseudocapacitance into the supercapacitor promoting the overall performance.[32, 33] The redox additives such as p-benzenediol (hydroquinone)[31, 34], *p*-phenylenediamine[35], NaI/I_2[32, 36], Potassium iodide (KI)[20], $VOSO_4$[37], indigo carmine[38, 39], ionic liquid[29, 40, 41] etc. were used with PVA/acid or base electrolyte to enhance the supercapacitive performance of the electrodes. In this work we introduced ionic liquid (IL) as a redox mediator with PVA/H_3PO_4 gel polymer electrolyte; since ILs have excellent thermal and electrochemical stability, non-volatility, non-flammable, and a few ILs are in a liquid state at room temperature. Furthermore, ILs has a wide working voltage range and so the SCs can operate at a large potential window with high energy density[42-44].

Here we applied ionic liquid, 1-ethyl-3-methylimidazolium tetrafluoroborate ([EMIM]BF_4) as a redox mediator in PVA/H_3PO_4 gel polymer electrolyte for AC/AC based supercapacitors. The addition of [EMIM]BF_4 in PVA/H_3PO_4 electrolyte shows an improvement in the ionic conductivity of the electrolyte and specific capacitance value. Different weight percentages of [EMIM]BF_4 (0, 25, 50, 75, 100 wt.%) content were substituted in PVA/H_3PO_4 electrolyte and the effect of electrochemical properties were studied using cyclic voltammetry (CV), galvanostatic charge-discharge (GCD), electrochemical impedance spectroscopy (EIS). The appropriate percentage of [EMIM]BF_4 in PVA/H_3PO_4 electrolyte effectively enhanced the specific capacitance value of the SC nearly up to 3 fold.

Experimental

Materials

For polymer electrolytes, poly(vinyl alcohol) (PVA) molecular weight of 130,000 g mol^{-1} was purchased from Sigma-Aldrich (USA), phosphoric acid (H_3PO_4, 85%) was obtained from Merck and 1-ethyl-3-methylimidazolium tetrafluoroborate ([EMIM]BF_4, 98%) was purchased from Alfa-Aesar (Korea). For the electrode, the activated carbon (BET ~820 m^2g^{-1}) was purchased from DAEJUNG Chemicals & Metals Co. Ltd (Korea), carbon black, poly(vinylidene fluoride) (PVDF) and N-methyl-2-pyrrolidone (NMP) were obtained from Alfa Aesar (Korea) and nitric acid purchased from SAMCHUN Chemicals (Korea).

Synthesis of polymer electrolyte

0.5 g of PVA was dissolved in distilled water (5 mL) at 80 °C under constant stirring for 2 h. After attaining clear PVA gel solution, 25, 50, 75, 100 wt.% (with respect to the weight of phosphoric acid) of [EMIM]BF_4 was added to this PVA gel solution and stirred for 2 h at the same temperature. Finally, the phosphoric acid of 0.8 g (160 wt. %) was added to the PVA/IL solution, stirred for few minutes and the temperature was lowered to 50 °C and stirred overnight. The photograph of as prepared gel polymer electrolytes and the dried PVA/H_3PO_4/IL electrolyte film are shown in Fig. 1 (a) and (b).

Fabrication of activated carbon electrode and supercapacitor

As purchased activated carbon (AC) was functionalized in nitric acid to enhance the capacitive performance[45, 46]. The functionalization was carried out by mixing 1 g of activated carbon in 100 mL of 1 M nitric acid solution and refluxed at 90 °C overnight. Then the acid treated AC was washed several times using distilled water until it attained neutral pH and then dried in vacuum at 100 °C overnight. The SC electrodes were fabricated by mixing 70 wt.% of functionalized AC, 20 wt.% of carbon black, 10 wt.% of PVDF and dispersed in NMP to produce a homogeneous slurry and then it was coated onto a stainless steel plate (1×1 cm^2). Finally, the fabricated electrodes were dried overnight at 50 °C in a vacuum oven. The average mass of loaded activated carbon in each electrode is ~1 mg. The photographic image of as fabricated electrodes is shown in Fig. 1 (c).

For supercapacitor fabrication, two activated carbon electrodes were dipped in the PVA electrolyte for 10 minutes at 80 °C and dried on the hot plate at 40 °C for 1 h. After drying excess water in the electrolyte, the consecutive electrodes were sandwiched face-to-face and sealed using vacuum tape to form a full cell. Finally, this supercapacitor was dried at 30 °C in a vacuum oven overnight. Fig. 1 (d) and (e) show the photographs of the SC and cross-sectional optical microscopic image of the fabricated SC.

Characterizations

The ionic conductivity of gel polymer PVA/H_3PO_4/IL electrolytes was measured using conductivity meter (COND 3110, WTW Company, Germany). Moreover, the ionic conductivities of dried polymer gel electrolytes were measured by placing the polymer films in between two stainless steel plates and testing the impedance using ZIVE SP2 workstation (Korea) at room temperature (~25 °C). Ionic conductivity (σ, Scm^{-1}) was calculated as per the following equation:

$$\sigma = \mathrm{t}/\mathrm{R}_b \times \mathrm{A} \qquad (1)$$

where, t (cm) is the thickness of the film between two stainless steel plates, A (cm^2) is the contact area of the electrolyte, R_b (ohm) is the bulk resistance obtained from the first intercept on the x-axis of the impedance data in the complex plane. Attenuated total reflectance - Fourier Transform Infrared Spectroscopy (ATR-FTIR) measurements were analysed using ATR-FTIR spectrometer (Smiths Detection, UK). Electrochemical measurements such as cyclic voltammetry (CV), galvanostatic charge-discharge (GCD) tests were performed at room temperature (~25 °C) by use of a ZIVE-SP2 (Korea) electrochemical workstation. The electrochemical experiments were performed in full cell configuration for the entire gel polymer electrolyte based SCs.

The specific capacitance (C_{sp}) value was calculated from charge/discharge curves, according to following equation:

$$C_{sp} = \mathrm{I} \times \mathrm{dt}/dV \times m \qquad (2)$$

where, I (A) is the applied discharge current, m (g) is the total mass of electrode materials on both electrodes, dt (s) is the discharge time and dV (V) represents the potential window. Energy density (E, $Whkg^{-1}$), power density (P, Wkg^{-1}) were calculated from the equations given below:

$$\mathrm{E} = C_{sp} \times (dV)^2/2 \quad (3)$$

$$P = \mathrm{E}/\mathrm{d}t \times 3{,}600 \quad (4)$$

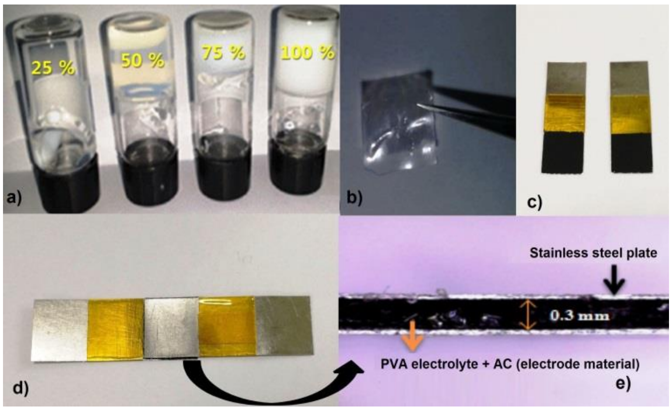

Fig. 1 (a) Photograph of $PVA/H_3PO_4/[EMIM]BF_4$ electrolytes, (b) $PVA/H_3PO_4/[EMIM]BF_4$ electrolyte film; (c) activated carbon electrodes; (d) fabricated full cell SC and (e) optical microscopic image of cross- section view.

Results and discussion

The presence of various functional groups of $PVA/[EMIM]BF_4$(50%) electrolyte was analysed using ATR-FTIR spectrum. Fig. 2 (a) shows the FTIR spectra of bare PVA, $[EMIM]BF_4$ and $PVA/[EMIM]BF_4$ gel polymer electrolyte. The spectrum of bare PVA shows a wide absorption band between 3550 and 3100 cm^{-1} representing the stretching vibration of O-H of the intermolecular and intramolecular hydrogen bonds. The band at 2942 and 2890 cm^{-1} corresponds to the stretching band of C-H from alkyl groups. The peak at 1415 cm^{-1} represents the bending vibration of the C-H bond and the absorption peak at 1140, 1087 and 835 cm^{-1} shows the symmetric C-C stretching mode or stretching of the C-O groups[47-49]. The resultant spectrum of $[EMIM]BF_4$ shows the characteristic vibrations peaks at 3164 and 3121 cm^{-1} that are assigned to the aromatic C-H stretching vibrations. The peak at 2985 and 1459 cm^{-1} represents the ethyl and methyl asymmetrical stretch and bending vibrations. The C=C stretch was observed at 1670 and 1574 cm^{-1} respectively. The sharp peak at 1164 cm^{-1} is assigned to the aromatic C-N vibration. The strong peak at 1058 cm^{-1} and short peak at 1285 cm^{-1} is assigned to the stretching vibration of BF present in the $[EMIM]BF_4$. Moreover the peak at 763 cm^{-1} corresponds to the asymmetric stretching vibration of BF_4 ions and the weak peaks around 763 to 890 cm^{-1} are the out-of-planar wagging vibrations of the rings[50-52]. In the case of the $PVA/[EMIM]BF_4$(50%) polymer, the spectrum shows the incorporation of IL in the PVA matrix with few characteristic peaks of IL at 3159, 3116, 1570, 1169 and 1053 cm^{-1} respectively. The spectrum shows slight shift in the peak positions, especially the skeletal and C-O stretching band of PVA from 835 to 841 cm^{-1} in the $PVA/[EMIM]BF_4$(50%) polymer indicating the stiffening of the polymer chain as a consequence of the interaction by H bonding between OH groups of PVA[48]. The FTIR spectrum of normal and functionalized activated carbon is shown in Fig. S1. The resultant spectrum confirms the enhancement of carboxylic functional groups in the functionalized activated carbon compared with the as purchased activated carbon.

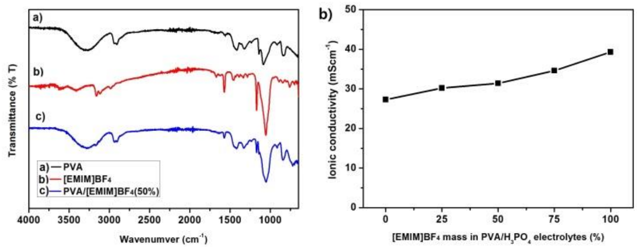

Fig. 2 (a) ATR-FTIR spectra of bare PVA, $[EMIM]BF_4$ and $PVA/[EMIM]BF_4$ (50%) polymer, (b) Ionic conductivity of PVA/H_3PO_4/IL polymer electrolyte at various wt.% of $[EMIM]BF_4$.

Fig. 2(b) shows the variation of ionic conductivity of PVA/H_3PO_4/IL gel polymer electrolyte with respect to various weight percentages of $[EMIM]BF_4$. The ionic conductivity of gel polymer electrolyte increases with inclusion of $[EMIM]BF_4$ from 27.3 $mScm^{-1}$ (PVA/H_3PO_4) to a maximum 39.3 $mScm^{-1}$ for 100 wt.% of $[EMIM]BF_4$ addition. The improved ionic conductivity is attributable to the plasticizing effect of the ionic liquid. This effect can effectivity soften the polymer backbone, enhance the flexibility of polymer chains and promote the ionic transportation in the polymer matrix.[41, 44, 53] Generally, the highly conducting polymer electrolyte has flexible polymer chains and it can boost up the mobility of the charge carriers to promote the ion dissociation in the polymer electrolytes. Moreover, the ionic conductivity of the polymer electrolytes is governed by the number of charge carriers, charge and mobility of carriers. In the case of PVA/H_3PO_4/IL, more charge carriers (imidazolium cation ($EMIM^+$) and BF_4^- ions) were induced in the polymer electrolyte in addition to the existing H_3O^+ and $H_2PO_4^-$ ions of H_3PO_4. Apart from the plasticizing effect, the incorporation of IL can effectively gain more charge carriers than PVA/H_3PO_4 polymer electrolytes and shows higher ionic conductivity.

The electrochemical properties of the as synthesized $PVA/H_3PO_4/[EMIM]BF_4$ polymer electrolytes were studied by utilizing carbon/carbon based supercapacitors. Fig. 3(a) shows the obtained cyclic voltammogram (CV) of supercapacitors with PVA/H_3PO_4 and various weight percentages of IL substituted polymer electrolytes measured at 5 mVs^{-1} scan rate. The supercapacitor using pure PVA/ H_3PO_4 electrolyte shows a typical rectangular shape CV curve; no peak due to Faradaic reaction was observed and representing the curve of an ideal electrical double layer capacitor.

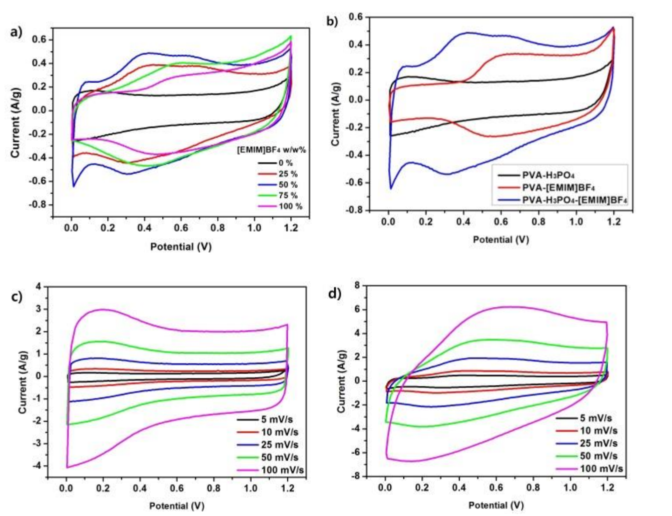

Figure 3 (a) Cyclic voltammogram of PVA/H_3PO_4, 25, 50, 75 and 100 wt. % [EMIM]BF_4 added PVA/H_3PO_4 polymer electrolyte based SCs at 5 mVs^{-1} scan rate; (b) CV curves of SCs with PVA/H_3PO_4, PVA/[EMIM]BF_4(50%) and PVA/ H_3PO_4/[EMIM]BF_4(50%) polymer electrolyte; (c) CV curves of PVA/H_3PO_4 electrolyte based supercapacitor for various scan rates and (d) CV curves of PVA/[EMIM]BF_4(50%) electrolyte based supercapacitor for various scan rates.

But, when [EMIM]BF_4 was added in PVA/H_3PO_4 electrolyte the supercapacitors show a pronounced background current with a distortion in the regular rectangular curve with a broad redox peak.[31] These peaks in the CV curve of PVA/H_3PO_4/[EMIM]BF_4 polymer electrolyte may be attributed to the redox process between the electrode/electrolyte interfaces owing to insertion/extraction reaction of [EMIM]BF_4 ions. To further corroborate this redox process, an experiment was performed with aqueous [EMIM]BF_4 electrolyte in a three-electrode cell. Fig. S2 shows the obtained CV curve that shows the oxidation and reduction process involved in the IL electrolyte, which is not exactly matched with the redox peak that was observed in the PVA/H_3PO_4/[EMIM]BF_4 polymer electrolyte based SCs. Moreover, Fig. 3(b) shows the CV curves of supercapacitors fabricated using PVA/H_3PO_4, PVA/[EMIM]BF_4(50%) and PVA/H_3PO_4/[EMIM]BF_4(50%) electrolytes. The CV of the supercapacitor based on PVA/H_3PO_4 electrolyte obviously shows a regular rectangular shape, but the PVA/[EMIM]BF_4(50%) supercapacitor displays distorted curves with redox peak confirming that pesudocapacitance occurred due to the existence of IL content in the electrolyte. Comparing the CV curves, the PVA/H_3PO_4/[EMIM]BF_4(50%) electrolytes based supercapacitor shows enhanced background current compared with the other two supercapacitors; with a broad redox peak. This was mainly ascribed to the enhanced ionic conductivity of these compositions with more charge carriers from both H_3PO_4 and [EMIM]BF_4.[54] Further, to examine the occurrence of the anomalous redox peak around 0.35 to 0.4 V, CV experiments were performed for the normal (as purchased) activated carbon and functionalized activated carbon in 1 M H_2SO_4 electrolyte in a three-electrode system (Fig S3). Obviously, the functionalized AC shows a redox peak at ~0.4V representing the faradaic reaction that occurred, due to the presence of more oxygenated functional groups present in the sample than the normal AC. The redox mechanism is mainly associated with the carbonyl or quinone type group as:, $>C_xO + H^+ + e^- \rightarrow >C_xOH$, where $>C_xOH$ represents a phenol - or hydroquinone type complex and e^- is an electron[45, 55]. This reaction should make a partial contribution to the faradaic peak of the FCS electrode. Table S1 shows the calculated specific capacitance of normal and functionalized AC based electrodes representing the enhanced performance of the functionalized AC electrode. Moreover, the CV experiment was also implemented with PVA/H_3PO_4/[EMIM]BF_4(50%) polymer electrolyte in normal and functionalized AC electrode in a two-electrode configuration (Fig S4a and S4b). Similarly the functionalized AC based SC shows an enhanced redox peak that originated from the oxygenated surface of the activated carbon. But the peak was not observed in the pure PVA/H_3PO_4 electrolyte based SCs. Thus it is believed that the incorporation of IL in the PVA/H_3PO_4 electrolyte effectively enhances the redox reaction due to the presence of additional imidazolium cations.

In Fig. 3(a) specific currents of the CV curves increase with respect to the inclusion of IL content up to 50 wt. % of [EMIM]BF_4 and then tends to decrease beyond this limit. Even though 75 and 100 wt. % of [EMIM]BF_4 in PVA/H_3PO_4 electrolyte shows higher ionic conductivity, the overall electrochemical performance declined; this may be due to reduction of the pseudo-reaction and less affinity of electrolyte towards the electrode surfaces. For more understanding, a wettability test was performed and contact angle was measured on the electrode using individual electrolytes. Fig. S5 shows the obtained microscopic image of the contact angle of electrolyte/electrode surface measured after 5 min of experiment. Initially all the polymer gel electrolytes show nearly the same contact angle above 70° and after 5 min the angle decreased and attained a saturated level with low contact angle of 29 and 38° for 25 and 50% [EMIM]BF_4 based electrolytes respectively. These confirmed that 50% [EMIM]BF_4 based electrolyte with comparable ionic conductivity and improved wettability can increase the accessibility of the specific surface area of the electrode and enhance the supercapacitive performance[56-58]. Apart from these, the excess amount of BF_4^- ions present in the electrolyte can increase the viscosity of electrolyte and easily cross-link with PVA; which restricts the flow of ions in the polymer matrix [59-62]. This can be clearly observed in the electrolyte prepared with above 50% [EMIM]BF_4. Fig. S6 shows the photograph of 75 and 100% [EMIM]BF_4 based gel polymer electrolytes, highlighting the formation of white precipitate and, above this wt.% of [EMIM]BF_4, the electrolyte tends to completely curdle white, forming an opaque gel. From an overall perspective, 50 weight % of [EMIM]BF_4 in PVA/H_3PO_4 electrolyte can serve as an excellent redox mediated gel polymer electrolyte for supercapacitors. The CV curves obtained from the devices with PVA/H_3PO_4 and [EMIM]BF_4 (50%)/PVA/H_3PO_4 at various scan rates are shown in Fig. 3(c) and (d) respectively. The PVA/H_3PO_4 based SC shows nearly rectangular shape for various scan rates with an increase in current with respect to the increase in scan rate. But, $[EMIM]BF_4$(50%)/PVA/H_3PO_4 supercapacitor shows irregular shape with large background current compared with the bare PVA/H_3PO_4 based SC.

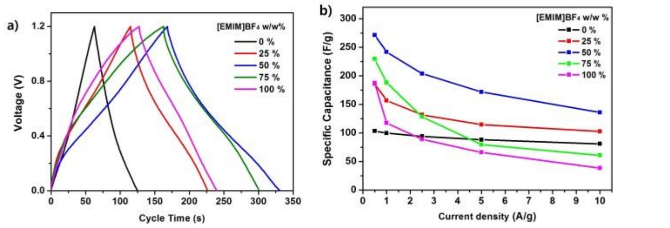

Fig. 4 (a) Galvanostatic charge/discharge curve of PVA/H_3PO_4 and $PVA/H_3PO_4/[EMIM]BF_4$ (25, 50, 75 and 100 wt. %) polymer gel electrolyte supercapacitors and (b) Variation of specific capacitance of SCs with respect to various discharge current densities.

The supercapacitive performances and specific capacitance values of the SCs fabricated with different combinations of polymer gel electrolytes were evaluated via galvanostatic charge/discharge tests for various discharge current densities (0.5 - 10 Ag^{-1}) over the potential window 0 - 1.2 V. Charge/discharge profiles of SCs based on PVA/H_3PO_4 and $PVA/H_3PO_4/[EMIM]BF_4$ (25, 50, 75 and 100 wt. %) polymer gel electrolyte at a constant discharge current density of 0.5 Ag^{-1} are shown in Fig. 4 (a). The curves for PVA/H_3PO_4 based SC display nearly typical symmetrical triangular shape, revealing that the capacitance originates from the electric double layer at the AC/electrolyte interfaces. In contrast $PVA/H_3PO_4/[EMIM]BF_4$ SC shows a slightly distorted triangle resembling the charge/discharge curves of pseudocapacitors[31, 63]. This confirms that the overall enhancement of electrochemical performance of SCs is due to the influence of the redox mediator $[EMIM]BF_4$ substituted in the PVA/H_3PO_4 gel polymer electrolyte. Similar to the CV curves the $PVA/H_3PO_4/[EMIM]BF_4$ (50%) SC shows a wider curve with extended discharge time; indicating a better supercapacitive performance from this combination. The specific capacitance values calculated from the resultant curves are 103, 186, 271, 229 and 187 Fg^{-1} for SCs based on PVA/H_3PO_4 and $PVA/H_3PO_4/[EMIM]BF_4$ (25, 50, 75 and 100 wt. %) electrolytes respectively. These evidence that the addition of $[EMIM]BF_4$ in PVA/H_3PO_4 can effectively increase the specific capacitance of the SCs to a larger extent due to the improved conductivity and occurrence of additional redox reaction in the device. The electrolyte with 50% of $[EMIM]BF_4$ shows a maximum specific capacitance value (271 Fg^{-1}) revealing the optimized level of IL incorporation in the electrolyte for better capacitive performance of SCs.

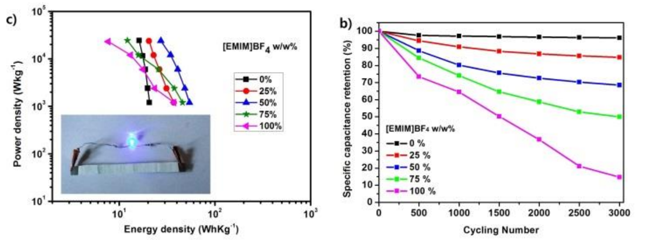

Fig. 5 (a) Ragone plot of supercapacitor based on polymer gel electrolytes; the inset picture showing that three SCs in series can lighten up a blue LED (2.2 V, ~10-20 mA) powered by 30 s charged SCs and (b) Cycling stability of the supercapacitor for 3000 cycles charging/discharging.

Fig. 4 (b) depicts the variation of calculated specific capacitance of SCs with respect to the various applied discharge current densities. The SC with 50% of $[EMIM]BF_4$ in PVA/H_3PO_4 gel polymer electrolyte shows excellent specific capacitance values of 136 - 271 Fg^{-1} for discharge current densities ranging from 10 to 0.5 Ag^{-1}. At the same time the bare PVA/H_3PO_4 based SC shows 80 - 103 Fg^{-1} specific capacitance values; confirming nearly or higher than 2 fold increment in the specific capacitance values due to the addition of $[EMIM]BF_4$ in PVA/H_3PO_4 gel polymer electrolyte. Moreover, the drop in specific capacitance of the SCs with increase in current densities is mainly due to the less involvement of the active materials, since at high current density the concentration of polarization at the electrode/electrolyte interface and diffusion rate of ions to the electrodes are not fast enough to meet the redox behavior, which decrease the rate of the reaction as well as double layer capacitance [64].

Fig. 5 (a) shows the Ragone plot (energy density vs. power density) of fabricated SCs. The energy density of PVA/ $H_3PO_4/[EMIM]BF_4$ (50%) SCs increase from 27.2 $Whkg^{-1}$ to 54.3 $Whkg^{-1}$ while the power density decreases from 23.9 $kWkg^{-1}$ to 1.2 $kWkg^{-1}$. At the same time PVA/H_3PO_4 SCs shows lower energy densities (16.2 $Whkg^{-1}$ to 20.7 $Whkg^{-1}$) with nearly the same power densities (24.3 $kWkg^{-1}$ to 1.2 $kWkg^{-1}$). Similarly, other combinations of PVA/ $H_3PO_4/[EMIM]BF_4$ (25, 75 and 100%) also show higher energy densities (37.2, 45.9 and 37.5 $Whkg^{-1}$) and nearly similar power densities compared with bare PVA/H_3PO_4 SCs. Furthermore, the performance of $PVA/H_3PO_4/[EMIM]BF_4$ (50%) SC was verified by assembling three SCs in series, charging for 30 s, and then successfully powering a blue LED (2.2 V, 10-20 mA) of 5 mm diameter [inset of Fig. 5(a)]. LEDs emitted very bright light after 2 min and even glowed after 5 min, demonstrating the good power and energy densities of the fabricated SCs.

The cyclic stability of PVA/H_3PO_4 and PVA/H_3PO_4/[EMIM]BF4 (25, 50, 75 and 100%) SCs were investigated by continuous charge/discharge measurements over 3000 cycles [Figure 5(b)] at a constant current density of 5 Ag^{-1}. The PVA/H_3PO_4 SC showed good cycling stability with 96% retention of initial specific capacitance values after 3000 cycles. But the stability of $[EMIM]BF_4$ added PVA/H_3PO_4 electrolyte based devices decreases with respect to the increase in percentage of

[EMIM]BF_4, showing ~ 85, 70, 50 and 15% specific capacitance retention for 25, 50, 75 and 100% [EMIM]BF4 content respectively, after 3000 cycles. The decrease in specific capacitance with charge /discharge cycles is possibly mainly due to the increase in aggregation of IL in the pores and amorphous electroactive area of the electrode [29, 44, 65]. This can effectively reduce the redox process of the electrolyte and decrease the specific capacitance values. Moreover, the ionic conductivity of the electrolytes drops drastically with aging of the electrolyte. Fig. S7 shows the decay of ionic conductivity for completely dried PVA/H_3PO_4 and PVA/H_3PO_4/[EMIM]BF_4 (25, 50, 75 and 100%) based electrolytes. Thus excess amounts of [EMIM]BF_4 content in PVA/H3PO4 can effectively reduce the ionic conductivity by restricting the flow of charge carriers due to easy aggregation of IL in the polymer matrix (as represented in Fig. S6).

The obtained Nyquist plots for PVA/H_3PO_4 and PVA/H_3PO_4/[EMIM]BF_4 supercapacitors are shown in Fig. 6(a), inset of the figure shows the magnified image of the high frequency portion of the plot. The plots behave in a similar trend as those of a resistor at the high frequency region and as a pure capacitor at the low frequency region[66]. The resultant plots were analysed using ZView software on the basis of the electrical equivalent circuit shown in the inset of Fig. 6(a). Broadly, the frequency range of the Nyquist plot is divided into high, middle and low frequency regions. At the high frequency region, the non-zero intersect of the semicircle is explained based on the equivalent series resistance (R_s), it is the combination of the internal resistance of the electrode material, the interfacial resistance at the active material and substrate and the polymer electrolyte resistance[67, 68]. The obtained R_s values of 0, 25, 50, 75 and 100 wt.% [EMIM]BF_4 added PVA/H_3PO_4 polymer electrolyte SCs are 2.55, 2.40, 2.64, 2.74 and 2.91 Ω respectively. This clearly reveals that there is no significant change in R_s due to addition of [EMIM]BF_4 in the polymer electrolyte. The mid-frequency region of the plot exhibits a single semicircle which indicates the electrochemical charge transfer resistance (R_{ct}) at the electrode and electrolyte interface. It shows that R_{ct} values increases with higher content of [EMIM]BF_4 in the PVA/H_3PO_4 polymer electrolyte (0.29, 1.04, 3.14, 4.50 and 5.62 for 0, 25, 50, 75 and 100 wt. % of [EMIM]BF_4).The higher charge transfer resistance of [EMIM]BF_4 added electrolyte than the pure PVA/H_3PO_4 polymer electrolyte is mainly due to the involvement of the redox reaction of [EMIM]BF_4 during the electrochemical process. Even though the SCs show large R_{ct} values due to its participation in the redox reaction, it can enhance the capacitance, thus its contribution is considerable for practical application[69]. The spike at lower frequency of the plots exhibits an angle between 45° to 90° relative to the real axis, representing the diffusion control process of the electrode, which was fitted with a Warburg element Z_w. In the case of the PVA/H_3PO_4 SC the low frequency spike is nearly parallel to the imaginary axis representing the existence of dominated electric double layer capacitance of the SC [68]. On the other hand, the spike deviated from the imaginary axis (approximately 45°) with respect to increase in content of [EMIM]BF_4, demonstrating the development of additional pseudocapacitive behaviour in the SCs[70]. Due to the non-ideal behavior of the plot, two constant phase element CPE_{dl} and CPE_p were included in the circuit (for best fitted values) representing the double layer and the pseudo-capacitance involved in the fabricated SCs. From the fit the CPE_p values of SCs increases with [EMIM]BF_4 addition (0.00193, 0.0123, 0.0139, 0.0124 and 0.0121 Fcm^{-1} for 0, 25, 50, 75 and 100 wt.% of [EMIM]BF_4 in PVA/H_3PO_4 SC) and shows maximum value for 50 wt.% [EMIM]BF_4 added polymer electrolyte based SCs; confirming the best electrochemical performance of this electrolyte combination.

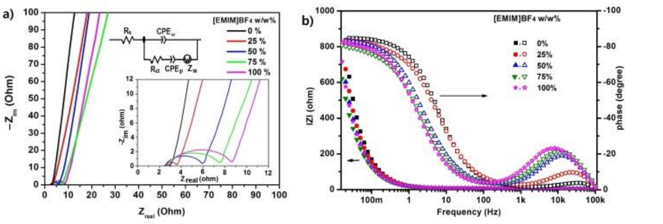

Fig. 6 (a) Nyquist plots for PVA/H_3PO_4 and PVA/H_3PO_4/[EMIM]BF_4 supercapacitors (inset shows the magnified portion of high frequency part of Nyquist plot and the equivalent circuit of fit) and (b) the Bode plot for the PVA/H_3PO_4 and PVA/H_3PO_4/[EMIM]BF_4 supercapacitors.

In addition, Bode plots of PVA/H_3PO_4 and PVA/H_3PO_4 /[EMIM]BF_4 SCs [Fig. 6(b)] indicated phase angles of SCs with different electrolyte combination between -81° and -85° at a frequency of 10 mHz, which is close to the 90° of an ideal capacitor, coinciding with the general RC equivalent circuit for supercapacitors[70]. The slightly lower phase angle of the PVA/H_3PO_4/[EMIM]BF_4 based SCs are due to the contribution of partial ideal capacitive behavior or the redox nature of the electrolyte in the SCs[71]. The PVA/H_3PO_4/[EMIM]BF_4 based SCs show a broad peak (ϕ) at low frequency region, which shifted to high frequency region with respect to increase in wt.% of [EMIM]BF_4 in electrolyte. This represents an increase in diffusion resistance of ions into the electrode[34, 72]. The large shift of the peak to higher frequency of the SCs with 75 and 100 wt. % [EMIM]BF_4 in the electrolyte may be due to the agglomeration of excess content IL in the electrolyte/electrolyte interface restricting the diffusion of ions into the electrodes. This might be the reason for the reduction of electrochemical performance of SCs with high wt.% of [EMIM]BF_4 in PVA/H_3PO_4 polymer electrolyte.

Conclusions

In summary, a novel redox-mediated gel polymer electrolyte based on PVA/H_3PO_4/ionic liquid (1-ethyl-3-methylimidazolium tetrafluoroborate, [EMIM]BF_4) have been utilized for the fabrication of functionalized activated carbon supercapacitors. The incorporation of appropriate content of [EMIM]BF_4 effectively increase the ionic conductivity, wettability and overall electrochemical performance of the supercapacitor. The electrochemical studies confirm that the induced redox reaction caused by the incorporation of $[EMIM]BF_4$ in PVA/H_3PO_4 polymer electrolyte is responsible for the overall enhancement of specific capacitance of the fabricated SCs. The electrolyte with 50 wt.% of $[EMIM]BF_4$ in PVA/H_3PO_4 demonstrated a maximum specific capacitance value of 271 Fg^{-1} and high energy density and power density of 54.3 $Whkg^{-1}$ and 23.9 $kWkg^{-1}$ respectively, with relatively comparable cyclic stability. Thus, the present work provides a promising prospect of utilizing the ionic liquid $[EMIM]BF_4$ as a redox mediator for gel polymer based electrolyte for the fabrication of high performance flexible or solid-state electrochemical supercapacitors.

Acknowledgements

The authors would like to acknowledge the authorities of Dongguk University-Seoul for their moral and financial support.

.

Notes and references

1. C. Peng, S. Zhang, X. Zhou and G. Z. Chen, *Energy Environ. Sci.,* 2010, **3**, 1499-1502.
2. A. Burke, *J. Power Sources,* 2000, **91**, 37-50.
3. R. Kotz and M. Carlen, *Electrochimi. Acta,* 2000, **45**, 2483-2498.
4. E. Frackowiak, *Phys. Chem. Chem. Phys.,* 2007, **9**, 1774-1785.
5. L. L. Zhang and X. S. Zhao, *Chem. Soc. Rev.,* 2009, **38**, 2520-2531.
6. Y. Zhu, S. Murali, M. D. Stoller, K. J. Ganesh, W. Cai, P. J. Ferreira, A. Pirkle, R. M. Wallace, K. A. Cychosz, M. Thommes, D. Su, E. A. Stach and R. S. Ruoff, *Science*, 2011, **332**, 1537-1541.
7. B. Kim, H. Chung and W. Kim, *Nanotech.*, 2012, **23**, 155401.
8. A. B. Fuertes and M. Sevilla, *ACS Appl. Mater. Interfaces*, 2015, **7**, 4344-4353.
9. G. Wang, L. Zhang and J. Zhang, *Chem. Soc. Rev.*, 2012, **41**, 797-828.
10. J. Park, B. Kim, Y. E. Yoo, H. Chung and W. Kim, *ACS Appl. Mater. Interfaces*, 2014, **6**, 19499-19503.
11. J. A. Lee, M. K. Shin, S. H. Kim, S. J. Kim, G. M. Spinks, G. G. Wallace, R. O.-Robles, M. D. Lima, M. E. Kozlov and R. H. Baughman, *ACS Nano*, 2012, **6**, 327–334.
12. C. J. Raj, B. C. Kim, W. J. Cho, W. G. Lee, S. D. Jung, Y. H. Kim, S. Y. Park and K. H. Yu, *ACS Appl. Mater. Interfaces*, 2015, **7**, 13405-13414.
13. R. Yuksel, Z. Sarioba, A. Cirpan, P. Hiralal and H. E. Unalan, *ACS Appl. Mater. Interfaces*, 2014, **6**, 15434-15439.
14. C. Zhao, C. Wang, Z. Yue, K. Shu and G. G. Wallace, *ACS Appl. Mater. Interfaces*, 2013, **5**, 9008-9014.
15. N. A. Choudhury, S. Sampath and A. K. Shukla, *Energy Environ. Sci.*, 2009, **2**, 55–67.
16. M. S. Kumar and D. K. Bhat, *J. Appl. Polym. Sci.*, 2009, **114**, 2445-2454.
17. G. Wang, X. Lu, Y. Ling, T. Zhai, H. Wang, Y. Tong and Y. Li, *ACS Nano*, 2012, **6**, 10296–10302.
18. S. K. Ujjain, V. Sahu, R. K. Sharma and G. Singh, *Electrochim. Acta*, 2015, **157**, 245-251.
19. H. Gao and K. Lian, *RSC Adv.*, 2014, **4**, 33091.
20. H. Yu, J. Wu, L. Fan, K. Xu, X. Zhong, Y. Lin and J. Lin, *Electrochim. Acta*, 2011, **56**, 6881-6886.
21. C. J. Raj and K. B. R. Varma, *Electrochim. Acta*, 2010, **56**, 649-656.
22. M. Singh, V. K. Singh, K. Surana, B. Bhattacharya, P. K. Singh and H.-W. Rhee, *J. Ind. Eng. Chem.*, 2013, **19**, 819-822.
23. I. Kuribayashi, M. Yamashita, S. Muraoka and K. Nagasawa, *J. Power Sources*, 1996, **63**, 121-125.
24. D. Peramunage, D. M. Pasquariello and K. M. Abraham, *J. Electrochem. Soc.*, 1995, **142**, 1789-1798.
25. M. Alamgir and K. M. Abraham, *J. Electrochem. Soc.*, 1993, **140**, L96-L97.
26. H. S. Choe, J. Giaccai, M. Alamgir and K. M. Abraham, *Electrochim. Acta*, 1995, **40**, 2289-2293.
27. B. Shen, J. Lang, R. Guo, X. Zhang and X. Yan, *ACS Appl. Mater. Interfaces*, 2015, **7**, 25378-25389.
28. C. Meng, C. Liu, L. Chen, C. Hu and S. Fan, *Nano Lett.*, 2010, **10**, 4025-4031.
29. C.-W. Liew, S. Ramesh and A. K. Arof, *Int. J. Hydrogen Energy*, 2014, **39**, 2953-2963.
30. Q. Chen, X. Li, X. Zang, Y. Cao, Y. He, P. Li, K. Wang, J. Wei, D. Wu and H. Zhu, *RSC Adv.*, 2014, **4**, 36253-36256.
31. H. Yu, J. Wu, L. Fan, Y. Lin, K. Xu, Z. Tang, C. Cheng, S. Tang, J. Lin, M. Huang and Z. Lan, *J. Power Sources*, 2012, **198**, 402-407.
32. J. Zhou, Y. Yin, A. N. Mansour and X. Zhou, *Electrochem. Solid-State Lett.*, 2011, **14**, A25.
33. S. T. Senthilkumar, R. K. Selvan and J. S. Melo, *J. Mater. Chem. A*, 2013, **1**, 12386-12394.
34. S. T. Senthilkumar, R. K. Selvan, N. Ponpandian and J. S. Melo, *RSC Adv.*, 2012, **2**, 8937-8940.
35. H. Yu, J. Wu, L. Fan, Y. Lin, S. Chen, Y. Chen, J. Wang, M. Huang, J. Lin, Z. Lan and Y. Huang, *Sci. China Chem.*, 2012, **55**, 1319-1324.
36. Y. Yin, J. Zhou, A. N. Mansour and X. Zhou, *J. Power Sources*, 2011, **196**, 5997-6002.
37. S. T. Senthilkumar, R. K. Selvan, N. Ponpandian, J. S. Melo and Y. S. Lee, *J. Mater. Chem. A*, 2013, **1**, 7913-7919.
38. S. Roldán, Z. González, C. Blanco, M. Granda, R. Menéndez and R. Santamaría, *Electrochim. Acta*, 2011, **56**, 3401-3405.
39. G. Ma, M. Dong, K. Sun, E. Feng, H. Peng and Z. Lei, *J. Mater. Chem. A*, 2015, **3**, 4035-4041.
40. Y.-S. Ye, J. Rick and B.-J. Hwang, *J. Mater. Chem. A*, 2013, **1**, 2719-2743.
41. C. W. Liew, S. Ramesh and A. K. Arof, *High Perform. Polym.*, 2014, **26**, 632-636.
42. M. Galiński, A. Lewandowski and I. Stępniak, *Electrochim. Acta*, 2006, **51**, 5567-5580.
43. D. Wei and T. W. Ng, *Electrochem. Commun.*, 2009, **11**, 1996-1999.
44. C.-W. Liew, S. Ramesh and A. K. Arof, *Int. J. Hydrogen Energy*, 2015, **40**, 852-862.
45. Y.-R. Nian and H. Teng, *J. Electrochem. Soc.*, 2002, **149**, A1008.

46. C. J. Raj, B. C. Kim, B. B. Cho, W. J. Cho, S. J. Kim, S. Y. Park and K. H. Yu, *Bull. Mater. Sci.*, 2016, **39**, 241–248.
47. H. S. Mansur, C. M. Sadahira, A. N. Souza and A. A. P. Mansur, *Mater. Sci. Eng. C*, 2008, **28**, 539-548.
48. S. Patachia, *Express Polym. Lett.*, 2011, **5**, 197-207.
49. H. S. Mansur, R. L. Oréfice and A. A. P. Mansur, *Polymer*, 2004, **45**, 7193-7202.
50. N. E. Heimer, R. E. Del Sesto, Z. Meng, J. S. Wilkes and W. R. Carper, *J. Mol. Liq.*, 2006, **124**, 84-95.
51. E. R. Talaty, S. Raja, V. J. Storhaug, A. Dolle and W. R. Carper, *J. Phys. Chem. B* 2004, **108**, 13177-13184.
52. S. A. Katsyuba, P. J. Dysonb, E. E. Vandyukova, A. V. Chernova and A. Vidisoe, *Helv. Chim. Acta*, 2004, **87**, 2556-2565.
53. C.-W. Liew, S. Ramesh and A. K. Arof, *Int. J. Hydrogen Energy*, 2014, **39**, 2917-2928.
54. S. T. Senthilkumar, R. K. Selvan, Y. S. Lee and J. S. Melo, *J. Mater. Chem. A*, 2013, **1**, 1086-1095.
55. H. Oda, A. Yamashita, S. Minoura, M. Okamoto and T. Morimoto, *J. Power Sources*, 2006, **158**, 1510-1516.
56. D. P. Dubal, S. H. Lee, J. G. Kim, W. B. Kim and C. D. Lokhande, *J. Mater. Chem.*, 2012, **22**, 3044.
57. M. Ma, C. Zhang, G. Huang, B. Xing, Y. Duan, X. Wang, Z. Yang and C. Zhang, *J. Nanomater.*, 2015, **2015**, 1-10.
58. B. Szubzda, A. Szmaja and A. Halama, *Electrochim. Acta*, 2012, **86**, 255-259.
59. M. Jiang, J. Zhu, C. Chen, Y. Lu, Y. Ge and X. Zhang, *ACS Appl. Mater. Interfaces*, 2016, **8**, 3473-3481.
60. E. Z. Casassa, A. M. Sarquis and C. H. Van Dyke, *J. Chem. Edu.*, 1986, **63**, 57-60.
61. H.-H. Wang, T.-W. Shyr and M.-S. Hu, *J. Appl. Polym. Sci.*, 1999, **74**, 3046–3052.
62. T. Itou, H. Kitai, A. Shimazu, T. Miyazaki and K. Tashiro, *J Phys Chem. B*, 2014, **118**, 6032-6037.
63. A. Vlad, N. Singh, S. Melinte, J. F. Gohy and P. M. Ajayan, *Sci. Rep.*, 2016, **6**, 22194.
64. S. Sathyamoorthi, V. Suryanarayanan and D. Velayutham, *J. Power Sources*, 2015, **274**, 1135-1139.
65. P. Jannasch, *Polymer*, 2001, **42**, 8692-8635.
66. C. Lei, N. Amini, F. Markoulidis, P. Wilson, S. Tennison and C. Lekakou, *J. Mater. Chem. A*, 2013, **1**, 6037.
67. Y. He, W. Chen, X. Li, Z. Zhang, J. Fu, C. Zhao and E. Xie, *ACS Nano*, 2013, **7**, 174-182.
68. J.-G. Wang, Y. Yang, Z.-H. Huang and F. Kang, *Carbon*, 2013, **61**, 190-199.
69. K. V. Sankar and R. K. Selvan, *RSC Adv.*, 2014, **4**, 17555-17566.
70. A. Di Fabio, A. Giorgi, M. Mastragostino and F. Soavi, *J. Electrochem. Soc.*, 2001, **148**, A845.
71. C. J. Hung, J. H. Hung, P. Lin and T. Y. Tseng, *J. Electrochem. Soc.*, 2011, **158**, A942.
72. C. Marino, A. Darwiche, N. Dupré, H. A. Wilhelm, B. Lestriez, H. Martinez, R. Dedryvère, W. Zhang, F. Ghamouss, D. Lemordant and L. Monconduit, *J. Phys. Chem. C*, 2013, **117**, 19302-19313.